Since January 2020 Elsevier has created a COVID-19 resource centre with free information in English and Mandarin on the novel coronavirus COVID-19. The COVID-19 resource centre is hosted on Elsevier Connect, the company's public news and information website.

Biosensors and Bioelectronics 237 (2023) 115439

Contents lists available at ScienceDirect

Biosensors and Bioelectronics

journal homepage: www.elsevier.com/locate/bios

Immunoaffinity biosensors for the detection of SARS-CoV-1 using screened Fv-antibodies from an autodisplayed Fv-antibody library

Jaeyong Jung [a], Ji-Hong Bong [a], Jeong Soo Sung [a], Jun-Hee Park [a], Tae-Hun Kim [a], Soonil Kwon [a], Min-Jung Kang [b], Joachim Jose [c], Jae-Chul Pyun [a,*]

[a] Department of Materials Science and Engineering, Yonsei University, 50 Yonsei-ro, Seodaemun-gu, Seoul, 03722, South Korea
[b] Korea Institute of Science and Technology (KIST), Seoul, South Korea
[c] Institute of Pharmaceutical and Medical Chemistry, Westphalian Wilhelms-University Münster, Münster, 48149, Germany

ARTICLE INFO

Keywords:
SARS-CoV-1
Spike protein
Fv-antibody library
Fv-antibody
SPR biosensor
Impedance spectrometry

ABSTRACT

The detection of severe acute respiratory syndrome coronavirus (SARS-CoV-1) was demonstrated using screened Fv-antibodies for SPR biosensor and impedance spectrometry. The Fv-antibody library was first prepared on the outer membrane of *E. coli* using autodisplay technology and the Fv-variants (clones) with a specific affinity toward the SARS-CoV-1 spike protein (SP) were screened using magnetic beads immobilized with the SP. Upon screening the Fv-antibody library, two target Fv-variants (clones) with a specific binding affinity toward the SARS-CoV-1 SP were determined and the Fv-antibodies on two clones were named "Anti-SP1" (with CDR3 amino acid sequence: ^{1}GRTTG^{5}NDRPD^{11}Y) and "Anti-SP2" (with CDR3 amino acid sequence: ^{1}CLRQA^{5}GTADD^{11}V). The binding affinities of the two screened Fv-variants (clones) were analyzed using flow cytometry and the binding constants (K_D) were estimated to be 80.5 ± 3.6 nM for Anti-SP1 and 45.6 ± 8.9 nM for Anti-SP2 (n = 3). In addition, the Fv-antibody including three CDR regions (CDR1, CDR2, and CDR3) and frame regions (FRs) between the CDR regions was expressed as a fusion protein (Mw. 40.6 kDa) with a green fluorescent protein (GFP) and the K_D values of the expressed Fv-antibodies toward the SP estimated to be 15.3 ± 1.5 nM for Anti-SP1 (n = 3) and 16.3 ± 1.7 nM for Anti-SP2 (n = 3). Finally, the expressed Fv-antibodies screened against SARS-CoV-1 SP (Anti-SP1 and Anti-SP2) were applied for the detection of SARS-CoV-1. Consequently, the detection of SARS-CoV-1 was demonstrated to be feasible using the SPR biosensor and impedance spectrometry utilizing the immobilized Fv-antibodies against the SARS-CoV-1 SP.

1. Introduction

Human coronaviruses (CoVs), such as CoV strains OC43, HKU1, NL63, and CoV-229E, are known to be among the most common etiologic agents for seasonal common colds and also pneumonia (Jain et al., 2015; Sariol and Perlman, 2020; Jung et al., 2021b). In particular, severe acute respiratory syndrome (SARS) has been reported to be caused by beta-CoV, as in the case of MERS and COVID-19 (Belouzard et al., 2012; Bong et al., 2020, 2021a; Chen et al., 2020; Elfiky, 2020; Jung et al., 2021a; Wuertz et al., 2021). SARS-associated coronavirus (SARS-CoV-1) infection has been reported to occur through binding of SARS-CoV-1 spike protein (SP) to the angiotensin-converting enzyme 2 (ACE2) receptor of the host cell (Lan et al., 2020; Sun et al., 2020). The receptor binding domain (RBD) of homotrimer spike glycoprotein is known to be the core region for the interaction between SP and ACE2, and the binding affinity of SP to ACE2 is known to be in the range of ~31–100 nM (Lan et al., 2020; Walls et al., 2020; Wrapp et al., 2020; Zahradník et al., 2021). Consequently, antibodies against the RBD region of the SP have been studied as potential therapeutic targets that can block viral entry to the host cell, and many research groups have reported the development of multiple high-affinity neutralizing antibodies against CoVs (He et al., 2006; Liu et al., 2020). For the detection of SARS-CoV-1 in medical samples, various kinds of detection methods have been used, such as PCR methods, immunoassays and so on. As summarized in Table 1, PCR methods have been used as a confirmatory test of infection because of its high sensitivity and the lateral flow immunoassay based on antibodies against SARS-CoV-1 SP have been widely used for the ease of detection without any instruments and rapid analysis time with a compromised sensitivity (Poon et al., 2004; Tahamtan and Ardebili, 2020; Oishee et al., 2021). For the development

* Corresponding author.
E-mail address: jcpyun@yonsei.ac.kr (J.-C. Pyun).

https://doi.org/10.1016/j.bios.2023.115439
Received 16 March 2023; Received in revised form 21 May 2023; Accepted 26 May 2023
Available online 27 May 2023

Table 1
Detection technologies for SARS-CoVs.

Detection method	Limit of detection	Sensitivity	Analysis time	Reference
Cell culture and microscopy	N/A	+++	1–2 days	(Farkash et al., 2020; Oishee et al., 2021)
Radiology-based detection	N/A	↔	10 min	(Peiris et al., 2003; Cozzi et al., 2020; Oishee et al., 2021)
Real-time RT-PCR	0.3–100 copies/μL Cut-off = 34–35 (Ct)	+++	1–2 h	(Lau et al., 2003; Tahamtan and Ardebili, 2020; Engelmann et al., 2021; Oishee et al., 2021)
RT-LAMP	5 copies/μL	+++	40 min	(Poon et al., 2004; Park et al., 2020; Oishee et al., 2021; Lino et al., 2022)
CRISPR-based diagnosis	10 copies/μL	+++	30–40 min	(Broughton et al., 2020; Oishee et al., 2021; Lee et al., 2022b; Lino et al., 2022)
ELISA/CLIA	↔	++	↔	(Bundschuh et al., 2020; Oishee et al., 2021)
Lateral flow immunoassay	↔	+	<20 min	(Quesada-González and Merkoçi, 2015; Oishee et al., 2021; Lino et al., 2022)
Electrochemical impedance spectroscopy	6 pg/mL	+++	<10 min	(Drobysh et al., 2022; Lino et al., 2022; Liustrovaite et al., 2022; Ong et al., 2023; Zukauskas et al., 2023)
Total internal reflection ellipsometry	0.3 nM (K_D)	+++	↔	(Qi et al., 2006; Drobysh et al., 2022; Plikusiene et al., 2022a, 2022b)
Field effect transistor	242 copies/μL	+++	↔	(Lino et al., 2022; Novodchuk et al., 2022)
Surface plasmon resonance	38.7 (Ct) (using Anti-SP2)	+++	<20 min	This work
Electrochemical impedance spectroscopy	38.2 (Ct) (using Anti-SP2)	+++	<10 min	This work

"+" Positive/Good; "++" Better; "+++" High; "↔" Variable; "−" Negative.

of a sensitive immunoassays including the lateral flow immunoassay, the screening of antibodies against SARS-CoV-1 with a high affinity to ACE2 has been a critical process (Lan et al., 2020; Sun et al., 2020).

This work presents the screening of Fv-antibodies against the SARS-CoV-1 SP from an Fv-antibody library, which was expressed on the outer membrane of *E. coli.* As shown in Fig. 1(a), Fv-antibody in this work represented the variable region of V_H-region which was composed of three CDR regions (CDR1, CDR2, and CDR3) and frame regions (FRs) in between the CDR regions (Xu and Davis, 2000). To prepare the Fv-antibody library, the amino acid sequence of the CDR3 region was randomized using site-directed mutagenesis, as shown in Fig. 1(b) (Xie et al., 2020). As previously reported (Jung et al., 2021c, 2021d; Lee et al., 2021; Sung et al., 2022a, 2022b), the Fv-antibody library plasmid was prepared based on anti-thyroid peroxidase (TPO) antibodies as a template sequence and the amino acid sequence of the CDR3 region (composed of eleven amino acids) was randomized and Fv-antibody library plasmids were prepared. As shown in Fig. 1(c), so-prepared Fv-antibody library plasmid was inserted into an authodisplay vector which expressed the Fv-antibody library on the outer membrane of *E. coli* (Jose and Meyer, 2007; Gratz et al., 2015). The control strain with the Fv-variant bearing the CDR1 and CDR2 regions was also prepared as the control. The efficiency of autodisplayed proteins have been reported to be as high as 10^5 proteins/*E. coli* (Jose and Meyer, 2007). And, the transformation was estimated to be occurred for more than 90% of total *E. coli* population (Yoo et al., 2015). Because of such a high expression efficiency of autodisplay technology, the target Fv-variants with a high affinity toward target antigens could be achieved without the need to perform the repeated biopanning process. So far various kinds of antibody libraries have been reported based on site-directed mutagenesis of IgG as summarized in Table 2. For example, the bacteriophage based antibody library has been the most frequently used among various libraries. In the case of the bacteriophage based antibody library was reported to have a transformation efficiency of <10 proteins/bacteriophage and <10% of total bacteriophage population (Pande et al., 2010). From such a low expression efficiency, the repeated biopanning process was inevitably required for the screening of target variants. Using the autodisplayed Fv-antibody library, several kinds of target Fv-variants have been screened against various antigens, such as biotin, dopamine, fluorescein, rhodamine B, and monosodium urate crystal, using an autodisplayed Fv-antibody library (Jung et al., 2021c, 2021d; Lee et al., 2021; Sung et al., 2022a, 2022b).

In comparison with the conventional IgG, the size of Fv-antibody (13.6 kDa) is far smaller than IgG (150 kDa). Such small antibodies or antibody fragments have been reported to have serval advantages for biosensor applications: (1) the small antibodies have a relatively high physico-chemial stability, such as high solubility, solvent-resistance and thermal tolerance (Kolkman and Law, 2010); (2) the small antibodies could be effectively used for transducers with a limited sensitive layer thickness, such as surface plasmon resonance (SPR) with the evanescence field in the range of 100–400 nm (Roper, 2007), field effect transistor (FET) with a Debye length of 0.7 nm (Chu et al., 2017), and electrochemical impedance spectroscopy (EIS) with an outer helmholtz plane (OHP) distance of <1.0 nm (Nakamura et al., 2011; Zhao et al., 2022); (3) the small antibodies could be effectively screened from antibody libraries for the antigens with a molecular weight of less than 5 kDa which had a low immunogenicity (Andorko et al., 2017; Jung et al., 2021d). As previously reported, the autodisplayed Fv-antibody library presented the feasibility of screening Fv-antibodies against various small antigens and biomarkers, such as dopamine for Parkinson's disease (Sung et al., 2022b), food allergens (Sung et al., 2022a), and monosodium urate crystal for gout (Jung et al., 2021c); (4) the small antibodies could be screened and produced in a short time in comparison with the antibody production using animal immunization (Fridy et al., 2014).

In this work, Fv-variants (clones) with a high affinity toward the SARS-CoV-1 SP were screened from the Fv-antibody library and the binding affinities of the two screened clones were analyzed using flow cytometry. And the, the screened Fv-antibodies against SARS-CoV-1 SP (Anti-SP1 and Anti-SP2) were expressed as a fusion protein with green fluorescence protein (GFP). Finally, the detection of SARS-CoV-1 was demonstrated for viral cultures of SARS-CoV-1 using the SPR biosensor and impedance spectrometry utilizing the immobilized Fv-antibodies obtained from the two screened clones against SARS-CoV-1 SP.

2. Experimental

2.1. Materials

SARS-CoV-1 SP (recombinant with amino acid residues of 14–667, 72.9 kDa) was supplied from Optolane Inc. (Seongnam, Korea). Luria-Bertani (LB) medium was purchased from Duchefa (Haarlem, Netherlands). M-280 tosyl-activated dynabead (diameter: 2.8 μm) was purchased from Invitrogen Co. (Carlsbad, CA, USA). Bovine serum albumin was purchased from Sigma-Aldrich Korea Seoul, Korea). Primers were custom-synthesized by Bionics (Seoul, Korea). Klenow DNA polymerase was purchaed from New England BioLabs (Ipswich, MA, USA). A PCR purification mini kit was purchased from Favorgen (Pingtug,

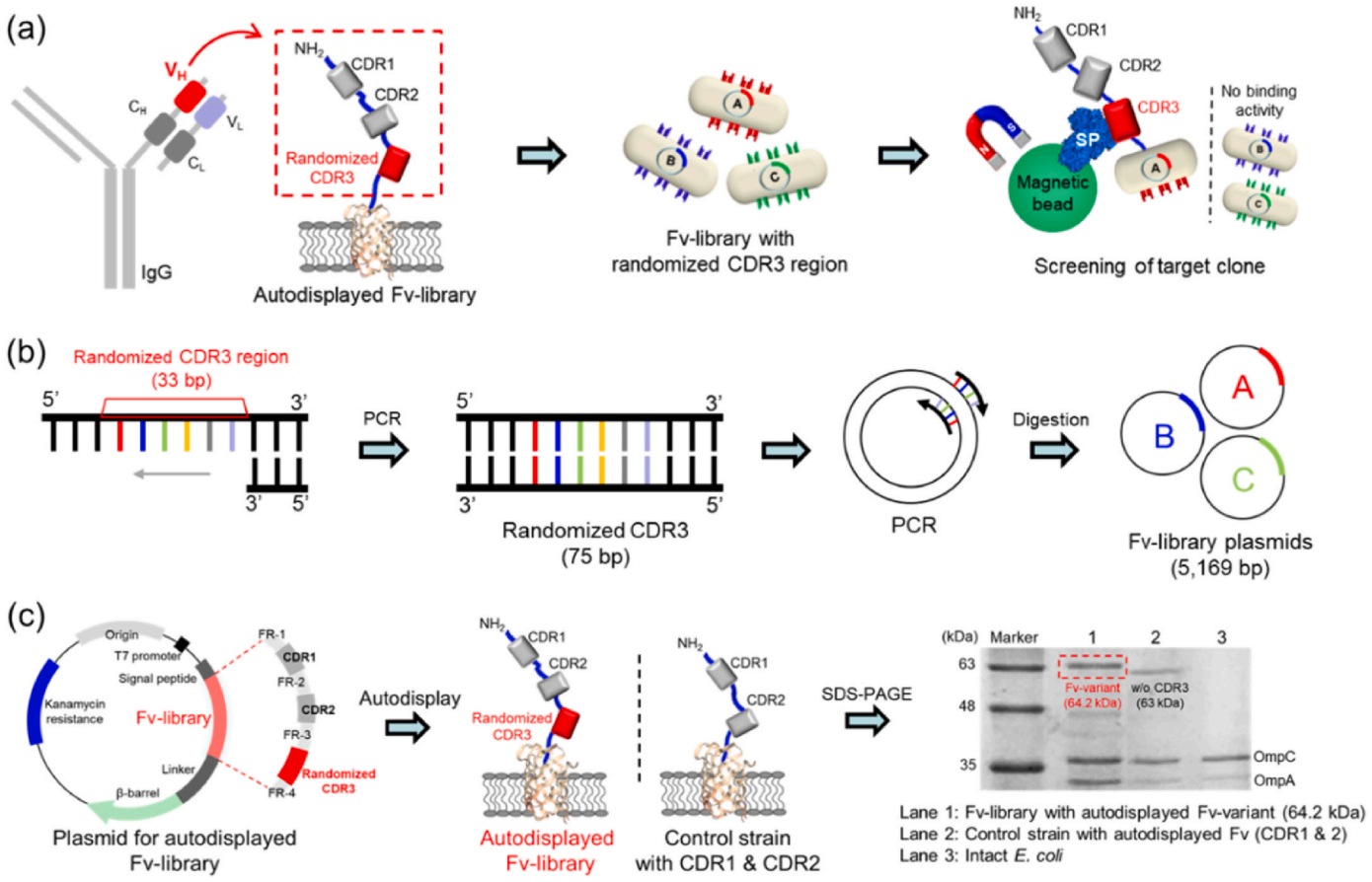

Fig. 1. Autodisplayed Fv-library with a randomized CDR3 region used for screening and the application of the Fv-variant used for the detection of SARS-CoV-1 using immunoaffinity biosensors. (a) Procedure for the screening of the Fv-variants from Fv-antibody library with randomized amino acid sequence at CDR3 region. (b) Preparation of the Fv-library with a randomized CDR3 region at V_H using site-directed mutagenesis. (c) Expression of the Fv-library on the outer membrane of *E. coli* using an autodisplay vector (SDS-PAGE of the autodisplayed Fv-variant, a control strain with CDR1 & CDR2, and intact *E. coli*).

Table 2
Antibody libraries based on protein engineering technologies.

Screening technology	Anchor protein	Surface density	Expression efficiency	Diversity of library	Screening method	Reference
E. coli autodisplayed library (This work)	AIDA-1	$> 10^5$ proteins/ *E. coli*	> 95%	$> 10^6$-10^7 clones	FACS (no biopanning)	Jose and Meyer (2007)
Anchored periplasmic expression	APEX	$> 10^5$ proteins/ *E. coli*	> 95%	$> 10^6$-10^7 clones	Biopanning (2–5 times)	Harvey et al. (2004)
Phage library	M13 gene III	< 10 proteins/ phage	> 10%	$> 10^7$ clones	Biopanning (2–5 times)	Pande et al. (2010)
Yeast library	Aga1-Aga2	10^4-10^5 proteins/ yeast	> 40%	$> 10^7$ clones	FACS (no biopanning)	(Linciano et al., 2019; Mei et al., 2019)

Taiwan). Phusion high-fidelity DNA polymerase was purchased from Thermo Fisher Scientific (Waltham, MA, USA). Plasmids for Fv-antibody labeled with green fluorescence protein (Superfolder GFP) (Liu et al., 2019; Kim et al., 2021) were custom-synthesized by Cosmogenetech (Seoul, Korea). Viral cultures were purchased from Zeptometrix (Buffalo, NY, USA): NATtrol^{TM} SARS-CoV-1 (Ct = 25–28), MERS-CoV (Ct = 25–28), CoV-229E strain reagent (Ct = 25–28) and NATtrol^{TM} negative control reagent (A-549 cells, 50,000 cells/mL) (; Jung et al., 2021a, 2021b; Wei et al., 2021; Park et al., 2022).

2.2. Autodisplay of the Fv-variants library

The Fv-antibody library was prepared and autodisplayed as previously reported (Jung et al., 2021c, 2021d; Lee et al., 2021; Sung et al., 2022a, 2022b). To prepare the Fv-antibody library with site-directed mutagenesis at the CDR3 region, the single-stranded forward primer with a randomized sequence of CDR3 (75 bp) was mixed with the corresponding reverse primer (22 bp), as shown in Fig. 1(b). The primer sequences for the Fv-antibody library are summarized in Table S1.

Subsequently, annealing of the primers (2 μL, respectively) was performed upon heating at 95 °C for 5 min, followed by cooling at 36 °C with NEB buffer (4 μL) and DW (32 μL) in a total volume of 40 μL. For the extension reaction, Klenow (exo-) DNA polymerase (3 μL), NEB buffer (16 μL), 10 mM dNTPs (8 μL), and distilled water (DW, 133 μL) were added to obtain a total volume of 200 μL.

Thereafter, the extension reaction was performed at 37 °C for 15 min. After inactivation of the enzyme reaction at 75 °C for 20 min, the PCP products (double-stranded primers of Fv-antibody library with a randomized CDR3 region) were filtered using a PCR purification mini kit. The Fv-antibody library plasmid with a randomized CDR3 sequence

was prepared using anti-thyroid peroxidase (TPO) antibodies as a template sequence. Fv-antibody library plasmids were synthesized using a template plasmid (pST009, 150 ng), double-stranded Fv-antibody library primer mixture (150 ng), HF buffer (10 μL), 10 mM dNTPs (1 μL), and Phusion high-fidelity DNA polymerase (0.5 μL) in a total volume of 50 μL. PCR was performed using the following steps: (1) Initial denaturation (98 °C for 1 min), (2) denaturation (98 °C for 30 s), (3) annealing (68 °C for 1 min), (4) elongation (72 °C for 5 min), (5) repetition of (2)–(4) for 30 cycles, and (6) termination (72 °C for 10 min). Finally, the template plasmids were digested using *Dpn*I restriction enzyme (37 °C for 16 h). The digested Fv-antibody library plasmids were filtered using a 100 K Amicon filter (Millipore, Billerica, MA, USA).The autodisplay of the Fv-antibody library on the outer membrane of *E. coli* BL21(DE3) was performed by transforming the prepared Fv-antibody library plasmid into competent intact cells via electroporation, as shown in Fig. 1(c) (Dower et al., 1988). The transformed *E. coli* cells were cultured in LB broth containing 50 μg/mL kanamycin at 37 °C for 16 h. The cultured *E. coli* cells (100 μL) were then cultured again in LB medium (10 mL) containing 99% β-mercaptoethanol (8 μL), kanamycin (50 μg/mL), and ethylenediaminetetraacetic acid (5 μM) at 37 °C with shaking (150 rpm) until it reached an OD_{600nm} of 0.6. To induce Fv-antibody library expression, the cultured *E. coli* cells (10 mL, $OD_{600nm} = 0.6$) were incubated with 1 mM isopropylthio-β-galactoside (IPTG) at 30 °C with shaking (120 rpm) for 3 h.

2.3. Screening of the target Fv-variants (clones)

Screening of the targeted *E. coli* with Fv-antibodies (Fv-variants) from the autodisplayed Fv-antibody library was performed using the following steps: (1) Fv-antibody library (500 μL, $OD_{600} = 0.5$) was reacted with M-280 tosyl-activated dynabeads (5 mg) coated with SARS-CoV-1 SP (20 μg) at 37 °C and 10 rpm for 1 h, (2) the target *E. coli*-bound magnetic beads were sorted using a magnet and the unbound *E. coli* were removed by rinsing the beads five times with 0.01% PBST and PBS, (3) the separated magnetic beads with bound *E. coli* against SARS-CoV-1 SP were resuspended in PBS (100 μL), and (4) the separated magnetic beads in PBS were spread on agar plates to obtain the screened *E. coli* clones, as shown in Fig. 2(b) (Jung et al., 2021b; Lamaiphan et al., 2021).

The binding properties of the screened *E. coli* clones against SARS-CoV-1 SP were estimated by mixing with FITC-labeled SARS-CoV-1 SP (Vira et al., 2010).

The screened *E. coli* (150 μL, $OD_{600} = 0.5$) were mixed with the FITC-labeled SARS-CoV-1 SP (3.1–100.0 nM) for 1 h. After centrifugation (3000×*g*, 2 min), the screened *E. coli* clones were washed with 0.01% PBST and PBS. After resuspension in PBS, the fluorescence intensity of screened clones was recorded using a FACSCalibur flow cytometer (Becton–Dickinson, Franklin Lakes, NJ, USA) operated at an excitation wavelength of 488 nm, as shown in Fig. 3.

2.4. Expression of the Fv-antibodies

The plasmids (pJY003 and pJY004), encoding an open reading frame of the Fv-antibody with binding activity toward the SARS-CoV-1 SP, fusion proteins were custom-synthesized by Cosmogenetech (Seoul, Korea), as shown in Fig. 4(a). The amino acid sequences of Fv-antibody consisted of CDRs and FRs were summarized in Table S2. The Fv-antibody was expressed intracellularly in *E. coli* by transforming the customized plasmid into competent cells. The transformed *E. coli* were cultured in 20 mL high-salt LB medium containing 1 mM IPTG and 30 μg/mL carbenicillin for 16 h at 30 °C. *E. coli* pellet was collected via centrifugation (3000×*g*, 3 min) and then resuspended in 50 mL of binding buffer (5 mM Tris-HCl, 0.5 mM EDTA, and 1 M NaCl) with 3 M urea. And then, the resuspended *E. coli* was sonicated using a sonic reactor (Vibra cell VCX-130, Sonics, USA). The lysate was centrifuged at

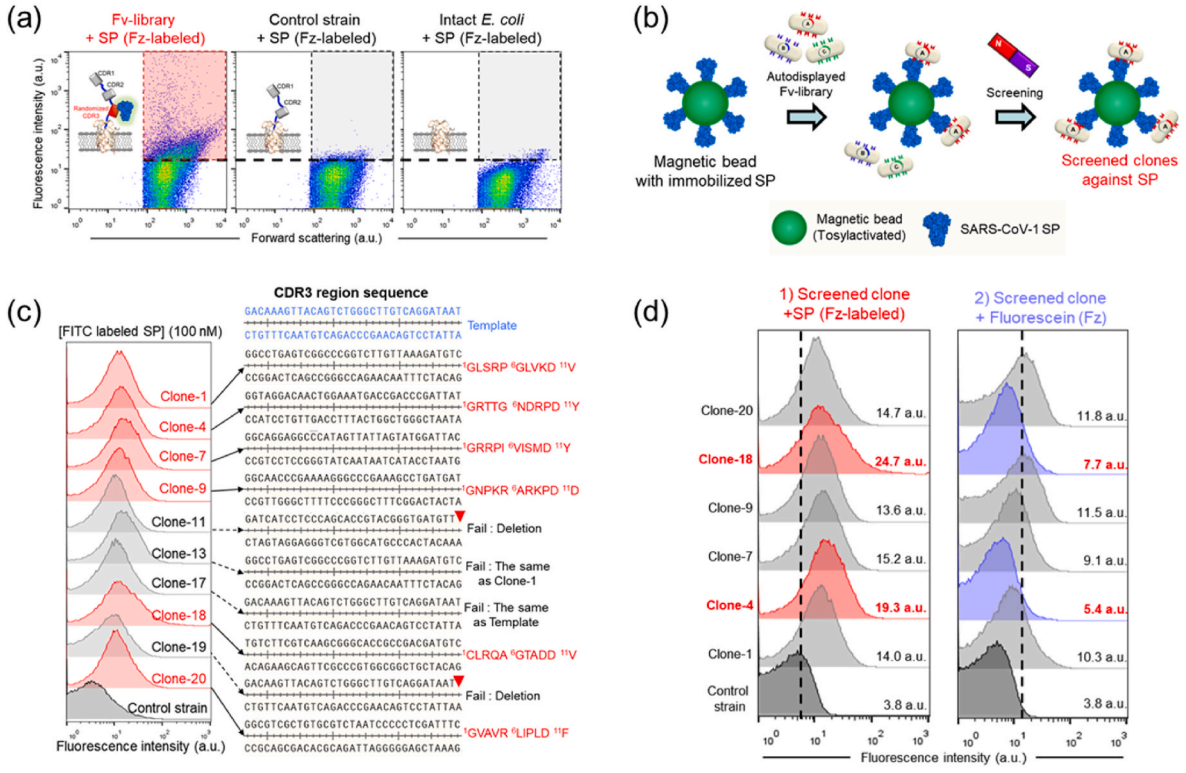

Fig. 2. Screening of the Fv-variants (clones) with affinity toward the spike SP of SARS-CoV-1. (a) Flow cytometric analysis after treatment of the fluorescence labeled SP to the Fv-antibody library, the control strain with CDR1, CDR2, and intact *E. coli*. (b) Screening procedure for the target clones using magnetic beads with immobilized SP. (c) Selection of the target clones using flow cytometry and genetic sequencing of the CDR3 region. (d) A comparison of the binding affinity of the screened clones to SP and fluorescence dye (fluorescein).

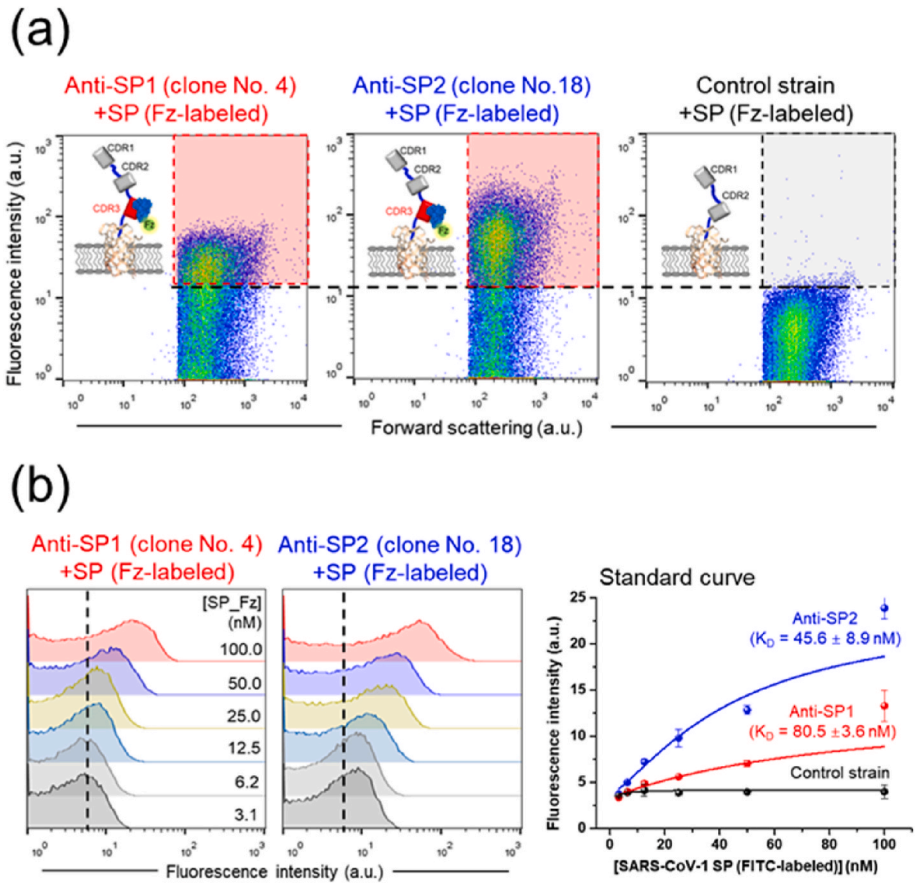

Fig. 3. Estimation of binding affinity of the screened clones. (a) Flow cytometric analysis after treatment of the fluorescence labeled SP with the screened clones compared with the control strain with CDR1 and CDR2. (b) Determination of the binding constant (K_D) using a quantitative binding assay with flow cytometry.

25,000×*g* for 10 min. The Fv-antibody in the supernatant was then purified on a His-tag purification column from Roche (Bassel, Switzerland) using elution buffer (binding buffer with 3 M urea and 500 mM imidazole) (Spriestersbach et al., 2015). The purified proteins were dialyzed for 16 h at 100 rpm and 4 °C to remove urea and imidazole.

2.5. SPR biosensor and impedance spectrometry utilizing the expressed Fv-antibodies

SPR measurements of the expressed Fv-antibodies obtained from Anti-SP1 and Anti-SP2 were estimated using an SPR biosensor from i-Cluebio (Seongnam, Korea). The assay configuration was prepared using the immobilized expressed Fv-antibodies or SARS-CoV-1 SP on the gold surface of the SPR biosensor. SPR chips for SPR measurements were prepared using the following steps: BK-7 glass (1 × 1 cm^2) was sputter coated with titanium, (thickness: 2 nm) as the adhesive layer, and gold (thickness: 48 nm). Fig. 4(b) and (c) show the SPR chips were incubated with the Fv-antibodies or SARS-CoV-1 SP (20 μg/mL, respectively) at 4 °C for 16 h. After washing with PBS, incubation for non-specific blocking with BSA (1 mg/mL) was performed for 1 h. After the washing step, a solution of the SARS-CoV-1 SP (3.8–30.0 nM) or Fv-antibodies (15.0–120.0 nM) solution was injected into the flow cell for 10 min (15 μL/min) as the association step. Finally, PBS was injected into the flow cell for 10 min (15 μL/min) as the dissociation step. The diluted NATtrol™ SARS-CoV-1, MERS-CoV, CoV-229E strain and negative samples in the dilution range of 100-fold (Ct value = 33.1) to 8000-fold (Ct value = 39.4) were analyzed in the same way as described using the SPR biosensor, as shown in Fig. 5(b). The SPR measurements were carried out by treating the samples under the flow conditions and the SPR signal according to the amount of bound analytes was recorded after the dissociation step (Jung et al., 2021d). The SPR signal was calculated as the dose-response curve for the samples with solution protein was carried out by the isotherm model:

$$R = \frac{R_{MAX}.[Ag]}{K_d + [Ag]}$$

where R represented the SPR signal (Rmax = maximum SPR signal), [Ag] represented the solution protein concentration and K_d represented affinity constant (Bong et al., 2020).

The results of SPR signals and impedance signals were fitted using Hill's equation.

$$y = \frac{a - d}{1 + \left(x/c\right)^2} + d$$

Where *a* and *d* were the maximum and minimum signals, respectively; *c* was the concentration of the solution protein; and *b* was the Hill's slope of the curve (Oshannessy et al., 1993; Saleviter et al., 2019; Lee et al., 2022a).

Impedance spectroscopy was carried out using a three-electrode system and commercial potentiostat from IVIUM Technologies (Eindhoven, Netherlands) (Bong et al., 2019; Patel et al., 2021; Jeong et al., 2022; Park et al., 2022). A gold electrode was prepared by sputtering a titanium layer (10 nm) as an adhesive layer and a gold layer (200 nm) on an SiO_2 wafer as a working electrode. Pt wire was used as a counter electrode for impedance spectroscopy. The reaction vessel was attached with a UV-curing glue to expose the working electrode area of 30 mm^2 (Bong et al., 2021b; Park et al., 2021; Song et al., 2022). The expressed Fv-antibodies (20 μg/mL) were immobilized on the electrode for 2 h. Incubation for non-specific blocking with BSA (1 mg/mL) was

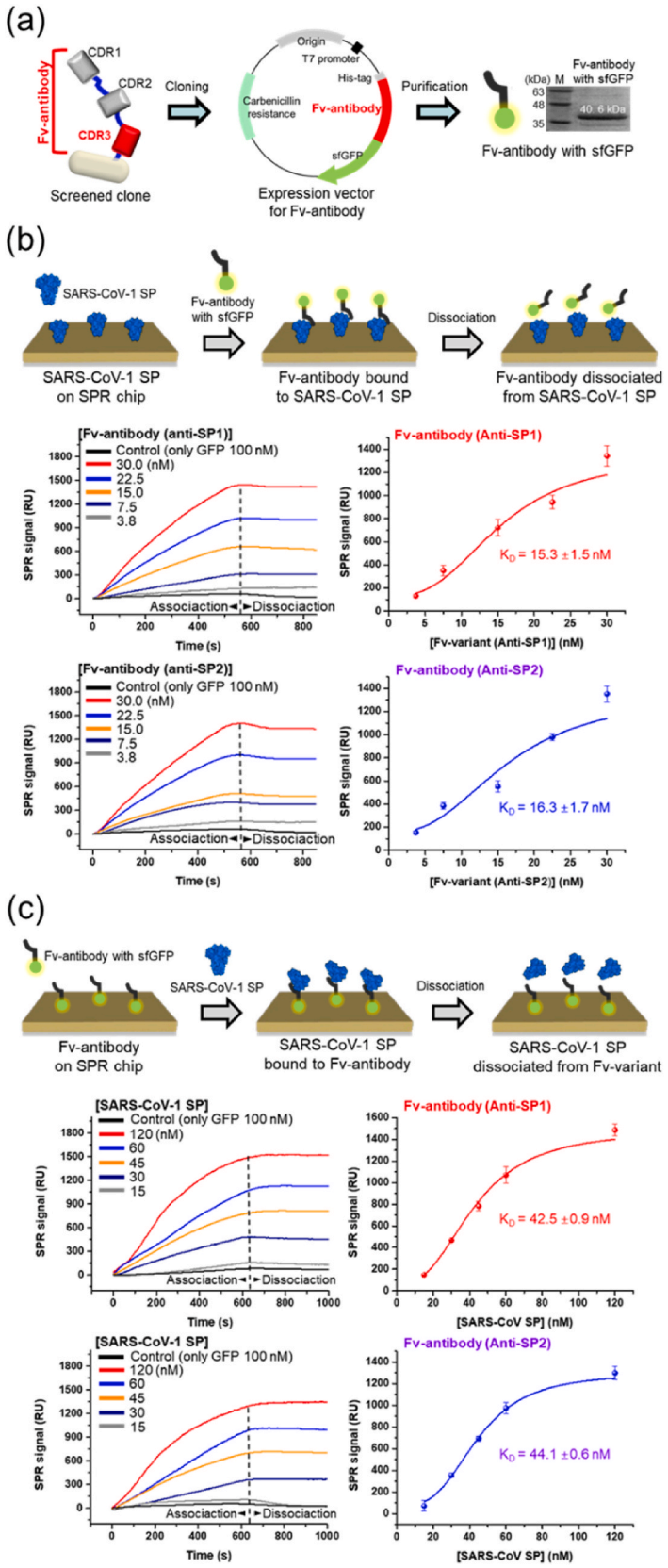

Fig. 4. Expression of the screened Fv-antibodies and estimation of the binding affinity. (a) Expression procedure for the screened Fv-antibodies. (b) Estimation of the binding constant (K_D) of the Fv-antibodies (Anti-SP1 and Anti-SP2) from two screened clones toward the immobilized SARS-CoV-1 SP using the SPR biosensor. (c) Estimation of the binding constant (K_D) of SARS-CoV-1 SP toward the immobilized Fv-antibodies using the SPR biosensor.

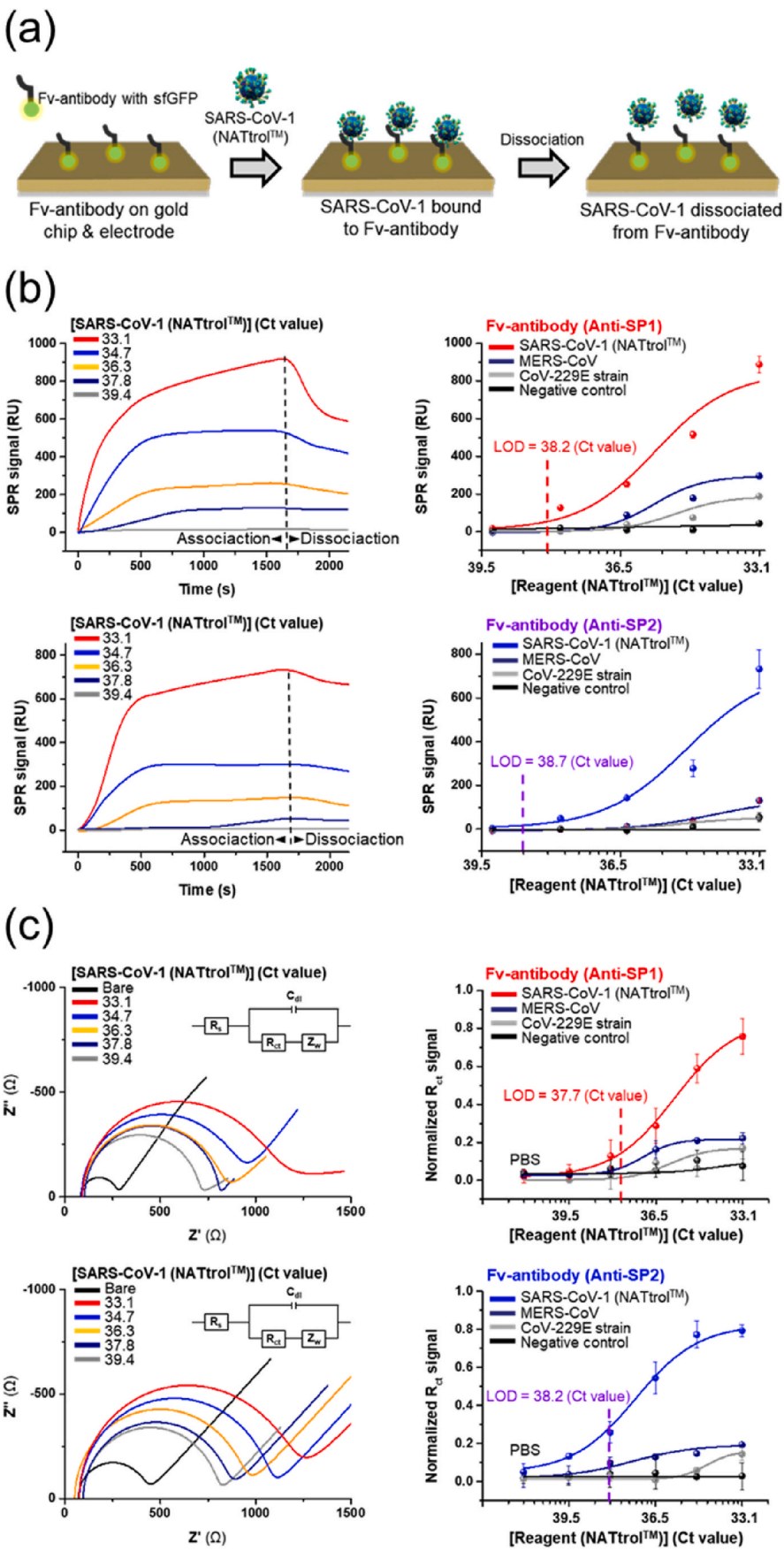

Fig. 5. Detection of SARS-CoV-1 using the SPR biosensor and impedance spectrometry. (a) Assay configuration of the SPR biosensor and impedance spectrometry with the immobilized Fv-antibodies (Anti-SP1 and Anti-SP2). (b) Detection of SARS-CoV-1 using the SPR biosensor with two kinds of immobilized Fv-antibodies (Anti-SP1 and Anti-SP2) from two screened clones. (c) Detection of SARS-CoV-1 using impedance spectrometry with two kinds of the screened Fv-antibodies (Anti-SP1 and Anti-SP2) from two screened clones.

performed on the electrode for 1 h. Diluted NATtrol™ SARS-CoV-1, MERS-CoV, CoV-229E strain and negative samples were added to the electrode and incubated for 30 min in the dilution range of 100-fold (Ct value = 33.1) to 8000-fold (Ct value = 39.4). Each detection was performed after a washing step with 0.01% PBST and PBS. Impedance spectroscopy was carried out in the frequency range of 0.1 Hz–1 MHz (amplitude: 10 mV) versus the Ag/AgCl reference electrode (amplitude: 50 mV) in potassium ferricyanide (50 mM), as shown in Fig. 5(c). The measured impedance value was performed using the Randles equivalent circuit model consisting of the parallel charge transfer resistance (R_{ct}) and a combination of double-layer capacitance (C_{dl}) with series medium resistance (R_s). The normalized charge transfer resistance (R_{ct}) signal was calculated by normalizing the change in R_{ct} after absorbing analyte on the electrode with the initial R_{ct} value of electrode. The calculation was performed as following equation: Normalized R_{ct} signal = $[R_{ct} - R_{ct0}]/R_{ct0}$, where R_{ct} was the value after the adsorption of analyte on the electrode and R_{ct0} was the initial R_{ct} value of the electrode (Bong et al., 2021b; Park et al., 2021)

3. Results and discussion

3.1. Screening of the Fv-antibodies against the SARS-CoV-1 SP

The Fv-antibody library with three CDR regions was prepared as previously reported by randomizing the CDR3 region (Jung et al., 2021c, 2021d; Lee et al., 2021; Sung et al., 2022a, 2022b). In addition, the control strain was also prepared with only CDR1 and CDR2 regions (without CDR3 region). After the fluorescence labeled SARS-CoV-1 SP was reacted to the Fv-antibody library, the control strain (with only CDR1 and CDR2), and intact *E. coli* (without autodisplayed Fv-antibodies), flow cytometric analysis was carried out and the resulting dot plots were compared with the Fv-antibody library. Fig. 2(a) showed that the Fv-antibody library exhibited a high fluorescence region on the dot plot when compared with that of the control strain (with only CDR1 and CDR2) and intact *E. coli* (without the autodisplayed Fv-antibodies) over the cut-off value (displayed as a dashed line in the graphs). In the case of the control strain and the intact *E. coli* only showed a fluorescence signal under the cut-off value.

Therefore, the high fluorescence region of the Fv-antibody library indicated that the CDR3 regions of some of the Fv-variants (clones) could bind to the fluorescence labeled SP with a high affinity. The Fv-variants (clones) with a specific affinity toward SP were screened from the autodisplayed Fv-antibody library on the outer membrane of *E. coli*. Fig. 2(b) showed that the SP was covalently immobilized on the tosyl-activated magnetic beads. Magnetic beads with the immobilized SP were incubated with the Fv-antibody library to screen Fv-variants (clones) with a binding affinity toward the SP. The magnetic beads with bound *E. coli* were isolated using an external magnet and then cultured on an agar plate. These clones were further analyzed to confirm that (1) the Fv-variants (clones) had a variated genetic sequence for the CDR3 region when compared with the template sequence, and (2) the Fv-variants (clones) had a specific affinity to the SP using the fluorescence labeled SP.

Among the cultured colonies on the agar plate, twenty colonies were randomly selected from the Fv-antibody library. Fig. 2(c) showed that the nucleotide sequences were analyzed for the randomized CDR3 region and six clones (Clone No. 1, 4, 7, 9, 18, and 20) were determined to have a binding affinity toward the fluorescence labeled SP, which had appropriate nucleotide sequences from the site-directed mutagenesis when compared with the template sequence. The other fourteen clones had inappropriate nucleotide sequences: Two clones were found to have deleted nucleotides, two clones had a repeated nucleotide sequence, and ten clones had the same nucleotide sequence as the template plasmid before site-directed mutagenesis. To investigate whether the binding of the fluorescence-labeled SP occurred at the fluorescence dye (fluorescein), the six selected clones (Clone No. 1, 4, 7, 9, 18, and 20) were reacted with the fluorescence-labeled SP as well as fluorescein dye. When the fluorescence dye (fluorescein) was reacted with the six selected clones, a remarkable fluorescence signal was observed for four clones (Clone No. 1, 7, 9, and 20), which indicated the non-specific binding of the fluorescence-labeled SP to these clones via the labeled fluorescence dye (fluorescein), as shown in Fig. 2(d). Two target clones with a specific binding affinity toward the SP were determined (Clone No. 4 and 18) and Fv-antibodies on two clones were named "Anti-SP1" for Clone No. 4 (amino acid sequence of CDR3 region: ^{1}GRTTG^{5}NDRPD^{11}Y) and "Anti-SP2" for Clone No. 18 (amino acid sequence of CDR3 region: ^{1}CLRQA^{5}GTADD^{11}V). The nucleotide sequences and corresponding amino acid sequences of the screened CDR3 regions were summarized in Table 3.

3.2. Binding properties of screened Fv-antibodies

The binding affinity of two screened Fv-variants (clones) was analyzed using flow cytometry. Initially, the fluorescence signals from the two screened clones were compared with the control strain (with only CDR1 and CDR2) after treatment with SARS-CoV-1 SP labeled with fluorescein. Fig. 3(a) showed the dot plots obtained for the two screened clones (Anti-SP1 and Anti-SP2) showed a far higher fluorescence signals when compared with the control strain. These results showed that the two screened clones had Fv-variants with a far higher affinity toward the SP via CDR3 regions.

To evaluate the binding constants (K_D) of the screened Fv-variants (clones), the fluorescence signal observed from the two screened clones were analyzed upon treatment with different concentrations of the fluorescein labeled SP. Fig. 3(b) showed the fluorescence signal was observed to quantitatively increase in the concentration range studied, and the signal observed for the control strain was maintained at the baseline level. To evaluate the K_D values of the Fv-variants (clones), the peak value was taken as the fluorescence signal. The dose-response curve was obtained by plotting the fluorescence signal with respect to the concentration of the fluorescence labeled SP. By fitting the dose-response curve using an isotherm model (Oshannessy et al., 1993; Saleviter et al., 2019; Bong et al., 2020), the K_D value was estimated to be 80.5 ± 3.6 nM for Anti-SP1 and 45.6 ± 8.9 nM for Anti-SP2 (n = 3) on the Fv-variants (clones). According to the literature, the K_D of SARS-CoV-1 SP toward the ACE2 receptor of the host was in the range of 31–100 nM (Lan et al., 2020; Walls et al., 2020; Wrapp et al., 2020; Zahradník et al., 2021). These results showed that the two screened Fv-variants (clones) had comparably high binding affinities toward the SARS-CoV-1 SP.

The Fv-antibodies including three CDR regions (CDR1, CDR2, and CDR3) and frame regions in-between the CDR regions were expressed as a fusion protein of GFP, as shown in Fig. 4(a). The GFP-fusion protein was carried out for the following reasons: (1) the Fv-antibody had a limited solubility and the fusion protein with GFP has a far improved solubility (Pédelacq et al., 2006; Liu et al., 2019) and (2) the GFP could be used effectively for the immobilization to the metal surface of biosensors. The immobilization efficiency of GFP was estimated to be similar to BSA which were frequently used as a blocking protein for immunoassays.

The binding of the expressed Fv-antibodies to the SP was monitored using the SPR sensor, which were associated and dissociated under

Table 3
Comparison of the amino acid sequence of the screened CDR3 regions.

Screened Fv-antibody	Sequence (11-amino acid)	Oligonucleotide sequence (33 base pairs)
Anti-SP1	N-^{1}GRTTG^{5}NDRPD^{11}Y–C	5′-GGT AGG ACA ACT GGAAAT GAC CGA CCC GAT TAT-3′
Anti-SP2	N-^{1}CLRQA^{5}GTADD^{11}V–C	5′-TGT CTT CGT CAA GCGGGC ACC GCC GAC GAT GTC-3′

continuous flow conditions. After the SP was immobilized on the SPR-chip, different concentrations of the expressed Fv-antibodies in the range of 3.8–30.0 nM were added, as shown in Fig. 4(b). The K_D values of the expressed Fv-antibodies toward the SP were estimated to be 15.3 ± 1.5 nM for the expressed Anti-SP1 and 16.3 ± 1.7 nM for the expressed Anti-SP2 (n = 3).

As the next step, the K_D values of the immobilized Fv-antibodies toward the SARS-CoV-1 SP were also estimated using the SPR biosensor for the application of the expressed Fv-antibodies to detect SARS-CoV-1. The expressed Fv-antibodies were immobilized on the SPR biosensor and different concentrations of the SARS-CoV-1 SP in the range of 15.0–120.0 nM were added, as shown in Fig. 4(c). The binding of the SP toward the expressed Fv-antibodies was monitored using the SPR sensor under the same continuous flow conditions and the K_D values of the expressed Fv-antibodies toward the SP were estimated to be 42.5 ± 0.9 nM for the expressed Anti-SP1 and 44.1 ± 0.6 nM for the expressed Anti-SP2 (n = 3). These results show that: (1) The binding constants for the immobilized Fv-antibodies to SPR were estimated to be in the nanomolar range and (2) the immobilized Fv-antibodies could be used for the detection of SARS-CoV-1. Additionally, the comparable binding constants (K_D values) of Fv-antibodies in comparison with those of native virus indicated that the Fv-antibody library could be effectively used for the screening of Fv-antibodies against various antigens related to other viral diseases.

3.3. Detection of SARS-CoV-1 using the expressed Fv-antibodies

The expressed Fv-antibodies (Anti-SP1 and Anti-SP2) obtained from the two screened clones against SARS-CoV-1 SP were used for the detection of SARS-CoV-1 using the SPR biosensor and impedance spectrometry. As a real sample of SARS-CoV-1, the NATtrol™ reagent of SARS-CoV-1 from Zeptometrix (Buffalo, NY, USA) was used, which was prepared with a similar composition to medical samples (Jung et al., 2021a, 2021b; Wei et al., 2021; Park et al., 2022). The cycle threshold (Ct) value of the NATtrol™ reagent was in the average range of 26.5 for SARS-CoV-1 (Wei et al., 2021; Park et al., 2022); the cut-off Ct value for the conventional diagnosis of SARS-CoV-1 using RT-PCR was reported to be 35 (Lau et al., 2003; Poon et al., 2003). In this work, standard samples for diagnosis using the SPR biosensor and impedance spectrometry were prepared upon serial dilution of the NATtrol™ reagent. As a negative control, NATtrol™ negative reagent without SARS-CoV-1 from Zeptometrix (Buffalo, NY, USA) was used in the SPR biosensor and impedance spectrometry.

Fig. 5(a) showed that the assay configuration for the detection of SARS-CoV-1 was prepared by immobilizing the expressed Fv-antibodies on the sensor surfaces of the SPR biosensor and gold electrode in the impedance spectrometer. SPR measurements were carried out upon treating the diluted SARS-CoV-1 samples obtained from the NATtrol ™ SARS-CoV-1 reagent in the average Ct range of 26.5 diluted in the range of 100-fold (Ct value = 33.1) to 8000-fold (Ct value = 39.4). Fig. 5(b) showed that the SPR measurements were carried out by treating the samples under flow conditions and the SPR signal according to the amount of bound analytes was recorded after the dissociation step. The detection of SARS-CoV-1 was possible in the dilution range of 100-fold (Ct value = 33.1) to 8000-fold (Ct value = 39.4); the SPR signal from the negative samples was maintained at the baseline level. The limit of detection was estimated to be the dilution factor of 3300-fold (Ct value = 38.2) for the Fv-antibodies (Anti-SP1) and 5000-fold (Ct value = 38.7) for the Fv-antibodies (Anti-SP2). These results show that the medical diagnosis of SARS-CoV-1 was feasible using the SPR biosensor with the screened antibodies (Anti-SP1 and Anti-SP2) against the SARS-CoV-1 SP.

Impedance spectrometry was carried out by treating the diluted SARS-CoV-1 samples in the same dilution range of 100-fold (Ct value = 33.1) to 8000-fold (Ct value = 39.4). Impedance spectrometry was carried out upon treating the samples under flow conditions and the impedance signal according to the amount of bound analytes was taken at the x-cut of the impedance spectrum after the washing step, as shown in Fig. 5(c). From the Nyquist plot (Fig. 5(c)), the signal of the charge transfer resistance (R ct) was taken from the fitting based on the Randles equivalent circuit model, which consisted of a parallel combination of double layer capacitance (C_{dl}) and charge transfer resistance (R_{ct}) with a series medium resistance (R_s). As previously reported (Park et al., 2021), the x-cut value represented the charge transfer resistance (R_{ct}), which indicated the resistance required for charge transfer to the electrode. Upon binding SARS-CoV-1, the R_{ct} value was observed to quantitatively increase, which indicated the specific binding of SARS-CoV-1 to the immobilized Fv-antibodies. The normalized charge transfer resistance (R_{ct}) signal was calculated by normalizing the change in R_{ct} after absorbing analyte on the electrode with the initial R_{ct} value of electrode. The calculation was performed as following equation: Normalized R_{ct} signal = $[R_{ct} - R_{ct0}]/R_{ct0}$, where R_{ct} was the value after the adsorption of analyte on the electrode and R_{ct0} was the initial R_{ct} value of the electrode (Bong et al., 2021b; Park et al., 2021). The detection of SARS-CoV-1 was possible in the range of 100-fold (Ct value = 33.1) to 8000-fold (Ct value = 39.4) and the impedance signal from the negative samples was maintained at the baseline level. The limit of detection was estimated to be 2500-fold (Ct value = 37.7) for the expressed Anti-SP1 and 3300-fold (Ct value = 38.2) for the expressed Anti-SP2. These results showed that the feasibility of medical diagnosis of SARS-CoV-1 using impedance spectrometry utilizing two screened Fv-antibodies (Anti-SP1 and Anti-SP2) against the SARS-CoV-1 SP. As summarized in Table 1, the LOD of this work was estimated to be Ct = 38.7 (with Anti-SP2) using SPR biosensor and Ct = 38.2 (with Anti-SP2) using impedance spectrometry. These results indicated that the LOD of this work was comparable to conventional real-time PCR methods which had the gold standard method for the diagnosis of SARS-CoVs with cutoff value of Ct = 34–35. Such a high level of LOD was estimated to be the high binding affinity (K_D) of the screened Fv-antibodies of Anti-SP1 (K_D = 15.3 nM) and Anti-SP2 (K_D = 16.3 nM) in comparison with the K_D of SARS-CoV-1 SP toward the ACE2 receptor of the host was in the range of 31–100 nM (Lan et al., 2020; Walls et al., 2020; Wrapp et al., 2020; Zahradník et al., 2021).

4. Conclusions

An Fv-antibody library was prepared on the outer membrane of *E. coli* using autodisplay technology. The Fv-variants with a specific affinity toward the SARS-CoV-1 SP were screened using paramagnetic beads immobilized with the SP. From the screening of the Fv-antibody library, two target clones with a specific binding affinity toward the SP were determined (Clone No. 4, and No. 18) and the screened Fv-antibodies were named “Anti-SP1” for Clone No. 4 (CDR3 amino acid sequence: ^{1}GRTTG^{5}NDRPD^{11}Y) and “Anti-SP2” for Clone No. 18 (CDR3 amino acid sequence: ^{1}CLRQA^{5}GTADD^{11}V). The binding affinities of the two screened clones were analyzed using flow cytometry. The fluorescence signal observed from these two screened clones were compared with the control strain with CDR1 and CDR2 only after treatment with SARS-CoV-1 SP labeled with fluorescein and the K_D value was estimated to be 80.5 ± 3.6 nM for Anti-SP1 and 45.6 ± 8.9 nM for Anti-SP2. From the literature, the binding affinity of SARS-CoV-1 SP to the ACE2 receptor of the host has been reported to be 31–100 nM. These results show that the two screened Fv-variants have a comparably high binding affinity toward the SARS-CoV-1 SP. And, the small size of Fv-antibodies indicated the feasibility of effective applications to transducers with a limited sensitive layer thickness, such as surface plasmon resonance (SPR), field effect transistor (FET) and electrochemical impedance spectroscopy (EIS). In addition, the Fv-antibodies including three CDR regions (CDR1, CDR2, and CDR3) and frame regions in-between the CDR regions were expressed as a fusion protein of sfGFP. The binding of the expressed Fv-antibodies toward the SP was monitored using the SPR sensor and the K_D values of the expressed Fv-antibodies toward the SP were estimated to be 15.3 ± 1.5 nM for the expressed Fv-antibodies

(Anti-SP1) and 16.3 ± 1.7 nM for the expressed Fv-antibodies (Anti-SP2) (n = 3). For the application of the expressed Fv-antibodies to detect SARS-CoV-1, the K_D values of the immobilized Fv-antibodies toward the SARS-CoV-1 SP were also estimated using the SPR biosensor. The assay results showed that: (1) The binding constants for the immobilized SARS-CoV-1 SP to the SPR were estimated to be in the nanomolar range and (2) the immobilized Fv-antibodies can be used for the detection of SARS-CoV-1. Finally, the expressed Fv-antibodies from the two screened clones against SARS-CoV-1 SP (Anti-SP1 and Anti-SP2) were applied for SARS-CoV-1 detection using the NATtrol™ reagent of SARS-CoV-1. The medical diagnosis of SARS-CoV-1 has been demonstrated to be feasible using the SPR biosensor as well as impedance spectrometry utilizing the immobilized Fv-antibodies obtained from the two clones screened against the SARS-CoV-1 SP.

Funding

Funding was received for this work.

Intellectual property

We confirm that we have given due consideration to the protection of intellectual property associated with this work and that there are no impediments to publication, including the timing of publication, with respect to intellectual property. In so doing we confirm that we have followed the regulations of our institutions concerning intellectual property.

Research ethics

We further confirm that any aspect of the work covered in this manuscript that has involved human patients has been conducted with the ethical approval of all relevant bodies and that such approvals are acknowledged within the manuscript.

Authorship

All listed authors meet the ICMJE criteria.
We attest that all authors contributed significantly to the creation of this manuscript, each having fulfilled criteria as established by the ICMJE.

We confirm that the manuscript has been read and approved by all named authors.

We confirm that the order of authors listed in the manuscript has been approved by all named authors.

Contact with the editorial office

This author submitted this manuscript using his/her account in EVISE.

We understand that this Corresponding Author is the sole contact for the Editorial process (including EVISE and direct communications with the office). He/she is responsible for communicating with the other authors about progress, submissions of revisions and final approval of proofs.

We confirm that the email address shown below is accessible by the Corresponding Author, is the address to which Corresponding Author's EVISE account is linked, and has been configured to accept email from the editorial office of American Journal of Ophthalmology Case Reports:

CRediT authorship contribution statement

Jaeyong Jung: Data curation, Investigation, Writing – original draft. **Ji-Hong Bong:** Investigation. **Jeong Soo Sung:** Investigation. **Jun-Hee Park:** Investigation. **Tae-Hun Kim:** Investigation. **Soonil Kwon:** Investigation. **Min-Jung Kang:** Supervision, Funding acquisition, Writing – original draft, Writing – review & editing. **Joachim Jose:** Supervision. **Jae-Chul Pyun:** Supervision, Funding acquisition, Writing – original draft, Writing – review & editing.

Declaration of competing interest

The authors declare that they have no known competing financial interests or personal relationships that could have appeared to influence the work reported in this paper.

Data availability

Data will be made available on request.

Acknowledgement

This work was supported by Korea Health Industry Development Institute (KHIDI) of Korea [HV22C0131] and the National Research Foundation (NRF) of Korea [RS-2023-00209053, NRF-2020R1A5A101913111 and NRF-2021R1A2C209370611].

Appendix A. Supplementary data

Supplementary data to this article can be found online at https://doi.org/10.1016/j.bios.2023.115439.

Abbreviations

SARS-CoV-1	severe acute respiratory syndrome coronavirus
SP	spike protein
CDR	complementarity determining region
ACE2	angiotensin-converting enzyme 2
RBD	receptor binding domain
FRs	frame regions
GFP	green fluorescence protein

References

Andorko, J.I., Pineault, K.G., Jewell, C., 2017. Impact of molecular weight on the intrinsic immunogenic activity of poly (beta amino esters). J. Biomed. Mater. Res. 105 (4), 1219–1229.

Belouzard, S., Millet, J.K., Licitra, B.N., Whittaker, G.R., 2012. Mechanisms of coronavirus cell entry mediated by the viral spike protein. Viruses 4 (6), 1011–1033.

Bong, J.-H., Kim, J., Lee, G.-Y., Park, J.-H., Kim, T.-H., Kang, M.-J., Pyun, J.-C., 2019. Fluorescence immunoassay of E. coli using anti-lipopolysaccharide antibodies isolated from human serum. Biosens. Bioelectron. 126, 518–528.

Bong, J.-H., Kim, T.-H., Jung, J., Lee, S.J., Sung, J.S., Lee, C.K., Kang, M.-J., Kim, H.O., Pyun, J.-C., 2020. Pig sera-derived anti-SARS-CoV-2 antibodies in surface plasmon resonance biosensors. BioChip. J. 14 (4), 358–368.

Bong, J.-H., Kim, T.-H., Jung, J., Lee, S.J., Sung, J.S., Lee, C.K., Kang, M.-J., Kim, H.O., Pyun, J.-C., 2021a. Competitive immunoassay of SARS-CoV-2 using pig sera-derived anti-SARS-CoV-2 antibodies. BioChip. J. 15, 1–9.

Bong, J.-H., Park, J.-H., Sung, J.S., Lee, C.K., Lee, G.-Y., Kang, M.-J., Kim, H.O., Pyun, J.-C., 2021b. Rapid analysis of bacterial contamination in platelets without pre-enrichment using pig serum-derived antibodies. ACS Appl. Bio Mater. 4 (11), 7779–7789.

Broughton, J.P., Deng, X., Yu, G., Fasching, C.L., Servellita, V., Singh, J., Miao, X., Streithorst, J.A., Granados, A., Sotomayor-Gonzalez, A., 2020. CRISPR–Cas12-based detection of SARS-CoV-2. Nat. Biotechnol. 38 (7), 870–874.

Bundschuh, C., Egger, M., Wiesinger, K., Gabriel, C., Clodi, M., Mueller, T., Dieplinger, B., 2020. Evaluation of the EDI enzyme linked immunosorbent assays for the detection of SARS-CoV-2 IgM and IgG antibodies in human plasma. Clin. Chim. Acta 509, 79–82.

Chen, Y., Liu, Q., Guo, D., 2020. Emerging coronaviruses: genome structure, replication, and pathogenesis. J. Med. Virol. 92 (4), 418–423.

Chu, C.-H., Sarangadharan, I., Regmi, A., Chen, Y.-W., Hsu, C.-P., Chang, W.-H., Lee, G.-Y., Chyi, J.-I., Chen, C.-C., Shiesh, S.-C., 2017. Beyond the Debye length in high ionic strength solution: direct protein detection with field-effect transistors (FETs) in human serum. Sci. Rep. 7 (1), 1–15.

Cozzi, D., Albanesi, M., Cavigli, E., Moroni, C., Bindi, A., Luvarà, S., Lucarini, S., Busoni, S., Mazzoni, L.N., Miele, V., 2020. Chest X-ray in new Coronavirus Disease 2019 (COVID-19) infection: findings and correlation with clinical outcome. Radiol. Med. 125, 730–737.

Dower, W.J., Miller, J.F., Ragsdale, C.W., 1988. High efficiency transformation of E. coli by high voltage electroporation. Nucleic Acids Res. 16 (13), 6127–6145.

Drobysh, M., Ramanaviciene, A., Viter, R., Chen, C.-F., Samukaite-Bubniene, U., Ratautaite, V., Ramanavicius, A., 2022. Biosensors for the determination of SARS-CoV-2 virus and diagnosis of COVID-19 infection. Int. J. Mol. Sci. 23 (2), 666.
Elfiky, A.A., 2020. Anti-HCV, Nucleotide Inhibitors, Repurposing against COVID-19. Life Sci., 117477
Engelmann, I., Alidjinou, E.K., Ogiez, J., Pagneux, Q., Miloudi, S., Benhalima, I., Ouafi, M., Sane, F., Hober, D., Roussel, A., 2021. Preanalytical issues and cycle threshold values in SARS-CoV-2 real-time RT-PCR testing: should test results include these? ACS Omega 6 (10), 6528–6536.
Farkash, E.A., Wilson, A.M., Jentzen, J.M., 2020. Ultrastructural evidence for direct renal infection with SARS-CoV-2. J. Am. Soc. Nephrol. 31 (8), 1683–1687.
Fridy, P.C., Li, Y., Keegan, S., Thompson, M.K., Nudelman, I., Scheid, J.F., Oeffinger, M., Nussenzweig, M.C., Fenyö, D., Chait, B.T., 2014. A robust pipeline for rapid production of versatile nanobody repertoires. Nat. Methods 11 (12), 1253–1260.
Gratz, A., Bollacke, A., Stephan, S., Nienberg, C., Le Borgne, M., Götz, C., Jose, J., 2015. Functional display of heterotetrameric human protein kinase CK2 on Escherichia coli: a novel tool for drug discovery. Microb. Cell Factories 14 (1), 1–13.
Harvey, B.R., Georgiou, G., Hayhurst, A., Jeong, K.J., Iverson, B.L., Rogers, G.K., 2004. Anchored periplasmic expression, a versatile technology for the isolation of high-affinity antibodies from Escherichia coli-expressed libraries. Proc. Natl. Acad. Sci. U. S.A. 101 (25), 9193–9198.
He, Y., Li, J., Du, L., Yan, X., Hu, G., Zhou, Y., Jiang, S., 2006. Identification and characterization of novel neutralizing epitopes in the receptor-binding domain of SARS-CoV spike protein: revealing the critical antigenic determinants in inactivated SARS-CoV vaccine. Vaccine 24 (26), 5498–5508.
Jain, S., Self, W.H., Wunderink, R.G., Fakhran, S., Balk, R., Bramley, A.M., Reed, C., Grijalva, C.G., Anderson, E.J., Courtney, D.M., 2015. Community-acquired pneumonia requiring hospitalization among US adults. N. Engl. J. Med. 373 (5), 415–427.
Jeong, H., Sharma, B., Jo, S., Kim, Y.H., Myung, J.-h., 2022. Electrochemical characteristics of La0. 8Sr0. 2MnO3 (LSM)–scandia-stabilized zirconia (ScSZ) composite cathode. J. Korean Ceram. Soc. 59 (4), 473–479.
Jose, J., Meyer, T.F., 2007. The autodisplay story, from discovery to biotechnical and biomedical applications. Microbiol. Mol. Biol. Rev. 71 (4), 600–619.
Jung, J., Bong, J.-H., Kim, H.-R., Park, J.-H., Lee, C.K., Kang, M.-J., Kim, H.O., Pyun, J.-C., 2021a. Anti-SARS-CoV-2 nucleoprotein antibodies derived from pig serum with a controlled specificity. BioChip. J. 15 (2), 195–203.
Jung, J., Bong, J.-H., Kim, T.-H., Sung, J.S., Lee, C., Kang, M.-J., Kim, H.O., Shin, H.-J., Pyun, J.-C., 2021b. Isolation of antibodies against the spike protein of SARS-CoV from pig serum for competitive immunoassay. BioChip. J. 15 (4), 396–405.
Jung, J., Bong, J.-H., Lee, S.J., Kim, M.-J., Sung, J.S., Lee, M., Kang, M.-J., Song, J., Jose, J., Pyun, J.-C., 2021c. Screening of Fv antibodies with specific binding activities to monosodium urate and calcium pyrophosphate dihydrate crystals for the diagnosis of gout and pseudogout. ACS Appl. Bio Mater. 4 (4), 3388–3397.
Jung, J., Bong, J.-H., Sung, J.S., Lee, S.J., Lee, M., Kang, M.-J., Jose, J., Pyun, J.-C., 2021d. Fluorescein and rhodamine B-binding domains from autodisplayed fv-antibody library. Bioconj. Chem. 32 (10), 2213–2223.
Kim, H., Hwang, S.G., Guk, K., Bae, Y., Park, H., Lim, E.-K., Kang, T., Jung, J., 2021. Development of antibody against drug-resistant respiratory syncytial virus: rapid detection of mutant virus using split superfolder green fluorescent protein-antibody system. Biosens. Bioelectron. 194, 113593.
Kolkman, J.A., Law, D.A., 2010. Nanobodies–from llamas to therapeutic proteins. Drug Discov. Today Technol. 7 (2), e139–e146.
Lamaiphan, N., Sakaew, C., Sricharoen, P., Nuengmatcha, P., Chanthai, S., Limchoowong, N., 2021. Highly efficient ultrasonic-assisted preconcentration of trace amounts of Ag (I), Pb (II), and Cd (II) ions using 3-mercaptopropyl trimethoxysilane-functionalized graphene oxide–magnetic nanoparticles. J. Korean Ceram. Soc. 58 (3), 314–329.
Lan, J., Ge, J., Yu, J., Shan, S., Zhou, H., Fan, S., Zhang, Q., Shi, X., Wang, Q., Zhang, L., Wang, X., 2020. Structure of the SARS-CoV-2 spike receptor-binding domain bound to the ACE2 receptor. Nature 581 (7807), 215–220.
Lau, L.T., Fung, Y.-W.W., Wong, F.P.-F., Lin, S.S.-W., Wang, C.R., Li, H.L., Dillon, N., Collins, R.A., Tam, J.S.-L., Chan, P.K., 2003. A real-time PCR for SARS-coronavirus incorporating target gene pre-amplification. Biochem. Biophys. Res. Commun. 312 (4), 1290–1296.
Lee, C.K., Jung, J., Kim, H.-R., Bong, J.-H., Kim, T.-H., Park, J.-H., Kwon, S., Kang, M.-J., Pyun, J.-C., 2022a. One-step immunoassay for the detection of food-poisoning related bacteria using a switching peptide. Analyst 147, 5363–5371.
Lee, S., Nam, D., Park, J.S., Kim, S., Lee, E.S., Cha, B.S., Park, K.S., 2022b. Highly efficient DNA reporter for CRISPR/Cas12a-Based specific and sensitive biosensor. BioChip. J. 1–8.
Lee, S.J., Bong, J.-H., Jung, J., Sung, J.S., Kang, M.-J., Jose, J., Pyun, J.-C., 2021. Screening of biotin-binding FV-antibodies from autodisplayed FV-library on E. coli outer membrane. Anal. Chim. Acta, 338627.
Linciano, S., Pluda, S., Bacchin, A., Angelini, A., 2019. Molecular evolution of peptides by yeast surface display technology. Medchemcomm 10 (9), 1569–1580.
Lino, A., Cardoso, M.A., Gonçalves, H.M., Martins-Lopes, P., 2022. SARS-CoV-2 detection methods. Chemosensors 10 (6), 221.
Liu, B., Shi, Y., Zhang, W., Li, R., He, Z., Yang, X., Pan, Y., Deng, X., Tan, M., Zhao, L., 2020. Recovered COVID-19 patients with recurrent viral RNA exhibit lower levels of anti-RBD antibodies. Cell. Mol. Immunol. 17 (10), 1098–1100.
Liu, M., Wang, B., Wang, F., Yang, Z., Gao, D., Zhang, C., Ma, L., Yu, X., 2019. Soluble expression of single-chain variable fragment (scFv) in Escherichia coli using superfolder green fluorescent protein as fusion partner. Appl. Microbiol. Biotechnol. 103 (15), 6071–6079.
Liustrovaite, V., Drobysh, M., Rucinskiene, A., Baradoke, A., Ramanaviciene, A., Plikusiene, I., Samukaite-Bubniene, U., Viter, R., Chen, C.-F., Ramanavicius, A., 2022. Towards an electrochemical immunosensor for the detection of antibodies against SARS-CoV-2 spike protein. JElS 169 (3), 037523.
Mei, M., Li, J., Wang, S., Lee, K.B., Iverson, B.L., Zhang, G., Ge, X., Yi, L., 2019. Prompting Fab yeast surface display efficiency by ER retention and molecular chaperon co-expression. Front. Bioeng. Biotechnol. 7, 362.
Nakamura, M., Sato, N., Hoshi, N., Sakata, O., 2011. Outer Helmholtz plane of the electrical double layer formed at the solid electrode–liquid interface. ChemPhysChem 12 (8), 1430–1434.
Novodchuk, I., Kayaharman, M., Prassas, I., Soosaipillai, A., Karimi, R., Goldthorpe, I., Abdel-Rahman, E., Sanderson, J., Diamandis, E., Bajcsy, M., 2022. Electronic field effect detection of SARS-CoV-2 N-protein before the onset of symptoms. Biosens. Bioelectron. 210, 114331.
Oishee, M.J., Ali, T., Jahan, N., Khandker, S.S., Haq, M.A., Khondoker, M.U., Sil, B.K., Lugova, H., Krishnapillai, A., Abubakar, A.R., 2021. COVID-19 pandemic: review of contemporary and forthcoming detection tools. Infect. Drug Resist. 14, 1049–1082.
Ong, V., Soleimani, A., Amirghasemi, F., Khazaee Nejad, S., Abdelmonem, M., Razaviyayn, M., Hosseinzadeh, P., Comai, L., Mousavi, M.P., 2023. Impedimetric sensing: an emerging tool for combating the COVID-19 pandemic. Biosensors 13 (2), 204.
Oshannessy, D.J., Brighamburke, M., Soneson, K.K., Hensley, P., Brooks, I., 1993. Determination of rate and equilibrium binding constants for macromolecular interactions using surface plasmon resonance: use of nonlinear least squares analysis methods. Anal. Biochem. 212 (2), 457–468.
Pande, J., Szewczyk, M.M., Grover, A.K., 2010. Phage display: concept, innovations, applications and future. Biotechnol. Adv. 28 (6), 849–858.
Park, G.-S., Ku, K., Baek, S.-H., Kim, S.-J., Kim, S.I., Kim, B.-T., Maeng, J.-S., 2020. Development of reverse transcription loop-mediated isothermal amplification assays targeting severe acute respiratory syndrome coronavirus 2 (SARS-CoV-2). J. Mol. Diagn. 22 (6), 729–735.
Park, J.-H., Bong, J.-H., Jung, J., Sung, J.S., Lee, G.-Y., Kang, M.-J., Pyun, J.-C., 2021. Microbial biosensor for Salmonella using anti-bacterial antibodies isolated from human serum. Enzym. Microb. Technol. 144, 109721.
Park, J.-H., Lee, G.-Y., Song, Z., Bong, J.-H., Chang, Y.W., Cho, S., Kang, M.-J., Pyun, J.-C., 2022. Capacitive biosensor based on vertically paired electrodes for the detection of SARS-CoV-2. Biosens. Bioelectron. 202, 113975.
Patel, S., Kodumudi Venkataraman, L., Yadav, H., 2021. Impedance and modulus analysis of barium calcium titanate ferroelectric ceramics. J. Korean Ceram. Soc. 58 (3), 337–350.
Pédelacq, J.-D., Cabantous, S., Tran, T., Terwilliger, T.C., Waldo, G.S., 2006. Engineering and characterization of a superfolder green fluorescent protein. Nat. Biotechnol. 24 (1), 79–88.
Peiris, J.S.M., Chu, C.-M., Cheng, V.C.-C., Chan, K., Hung, I., Poon, L.L., Law, K.-I., Tang, B., Hon, T., Chan, C., 2003. Clinical progression and viral load in a community outbreak of coronavirus-associated SARS pneumonia: a prospective study. Lancet 361 (9371), 1767–1772.
Plikusiene, I., Maciulis, V., Juciute, S., Maciuleviciene, R., Balevicius, S., Ramanavicius, A., Ramanaviciene, A., 2022a. Investigation and comparison of specific antibodies' affinity interaction with SARS-CoV-2 wild-type, B. 1.1. 7, and B. 1.351 spike protein by total internal reflection ellipsometry. Biosensors 12 (5), 351.
Plikusiene, I., Maciulis, V., Juciute, S., Ramanavicius, A., Balevicius, Z., Slibinskas, R., Kucinskaite-Kodze, I., Simanavicius, M., Balevicius, S., Ramanaviciene, A., 2022b. Investigation of SARS-CoV-2 nucleocapsid protein interaction with a specific antibody by combined spectroscopic ellipsometry and quartz crystal microbalance with dissipation. J. Colloid Interface Sci. 626, 113–122.
Poon, L.L., Chan, K.H., Wong, O.K., Yam, W.C., Yuen, K.Y., Guan, Y., Lo, Y.D., Peiris, J.S., 2003. Early diagnosis of SARS coronavirus infection by real time RT-PCR. J. Clin. Virol. 28 (3), 233–238.
Poon, L.L., Leung, C.S., Tashiro, M., Chan, K.H., Wong, B.W., Yuen, K.Y., Guan, Y., Peiris, J.S., 2004. Rapid detection of the severe acute respiratory syndrome (SARS) coronavirus by a loop-mediated isothermal amplification assay. Clin. Chem. 50 (6), 1050–1052.
Qi, C., Duan, J.-Z., Wang, Z.-H., Chen, Y.-Y., Zhang, P.-H., Zhan, L., Yan, X.-Y., Cao, W.-C., Jin, G., 2006. Investigation of interaction between two neutralizing monoclonal antibodies and SARS virus using biosensor based on imaging ellipsometry. Biomed. Microdevices 8, 247–253.
Quesada-González, D., Merkoçi, A., 2015. Nanoparticle-based lateral flow biosensors. Biosens. Bioelectron. 73, 47–63.
Roper, D.K., 2007. Determining surface plasmon resonance response factors for deposition onto three-dimensional surfaces. ChEnS 62 (7), 1988–1996.
Saleviter, S., Fen, Y.W., Daniyal, W.M.E.M.M., Abdullah, J., Sadrolhosseini, A.R., Omar, N.A.S., 2019. Design and analysis of surface plasmon resonance optical sensor for determining cobalt ion based on chitosan-graphene oxide decorated quantum dots-modified gold active layer. Opt Express 27 (22), 32294–32307.
Sariol, A., Perlman, S., 2020. Lessons for COVID-19 immunity from other coronavirus infections. Immunity 53 (2), 248–263.
Song, Z., Park, J.-H., Kim, H.-R., Lee, G.-Y., Kang, M.-J., Kim, M.-H., Pyun, J.-C., 2022. Carbon electrode obtained via pyrolysis of plasma-deposited parylene-C for electrochemical immunoassays. Analyst 147 (16), 3783–3794.
Spriestersbach, A., Kubicek, J., Schäfer, F., Block, H., Maertens, B., 2015. Purification of his-tagged proteins. Methods Enzymol. 1–15 (Elsevier).
Sun, C., Chen, L., Yang, J., Luo, C., Zhang, Y., Li, J., Yang, J., Zhang, J., Xie, L., 2020. SARS-CoV-2 and SARS-CoV Spike-RBD Structure and Receptor Binding Comparison and Potential Implications on Neutralizing Antibody and Vaccine Development (Biorxiv).

Sung, J.S., Bong, J.-H., Lee, S.J., Jung, J., Kang, M.-J., Lee, M., Shim, W.-B., Jose, J., Pyun, J.-C., 2022a. One-step immunoassay for food allergens based on screened mimotopes from autodisplayed FV-antibody library. Biosens. Bioelectron. 202, 113976.

Sung, J.S., Bong, J.-H., Yun, T.G., Han, Y., Park, Y., Jung, J., Lee, S.J., Kang, M.-J., Jose, J., Lee, M., 2022b. Antibody-Mediated screening of peptide inhibitors for monoamine oxidase-B (MAO-B) from an autodisplayed FV library. Bioconj. Chem. 33 (6), 1166–1178.

Tahamtan, A., Ardebili, A., 2020. Real-time RT-PCR in COVID-19 detection: issues affecting the results. Expert Rev. Mol. Diagn. 20 (5), 453–454.

Vira, S., Mekhedov, E., Humphrey, G., Blank, P.S., 2010. Fluorescent-labeled antibodies: balancing functionality and degree of labeling. Anal. Biochem. 402 (2), 146–150.

Walls, A.C., Park, Y.-J., Tortorici, M.A., Wall, A., McGuire, A.T., Veesler, D., 2020. Structure, function, and antigenicity of the SARS-CoV-2 spike glycoprotein. Cell 181 (2), 281–292. e286.

Wei, S., Suryawanshi, H., Djandji, A., Kohl, E., Morgan, S., Hod, E.A., Whittier, S., Roth, K., Yeh, R., Alejaldre, J.C., 2021. Field-deployable, rapid diagnostic testing of saliva for SARS-CoV-2. Sci. Rep. 11 (1), 1–9.

Wrapp, D., Wang, N., Corbett, K.S., Goldsmith, J.A., Hsieh, C.-L., Abiona, O., Graham, B. S., McLellan, J.S., 2020. Cryo-EM structure of the 2019-nCoV spike in the prefusion conformation. Science 367 (6483), 1260–1263.

Wuertz, K.M., Barkei, E.K., Chen, W.-H., Martinez, E.J., Lakhal-Naouar, I., Jagodzinski, L. L., Paquin-Proulx, D., Gromowski, G.D., Swafford, I., Ganesh, A., 2021. A SARS-CoV-2 spike ferritin nanoparticle vaccine protects hamsters against Alpha and Beta virus variant challenge. npj Vaccines 6 (1), 1–11.

Xie, S., Wang, J., Yu, X., Peng, T., Yao, K., Wang, S., Liang, D., Ke, Y., Wang, Z., Jiang, H., 2020. Site-directed mutations of anti-amantadine scFv antibody by molecular dynamics simulation: prediction and validation. J. Mol. Model. 26 (3), 1–9.

Xu, J.L., Davis, M.M., 2000. Diversity in the CDR3 region of VH is sufficient for most antibody specificities. Immunity 13 (1), 37–45.

Yoo, G., Saenger, T., Bong, J.-H., Jose, J., Kang, M.-J., Pyun, J.-C., 2015. Co-autodisplay of Z-domains and bovine caseins on the outer membrane of E. coli. Biochim. Biophys. Acta 1848 (12), 3126–3133.

Zahradník, J., Marciano, S., Shemesh, M., Zoler, E., Harari, D., Chiaravalli, J., Meyer, B., Rudich, Y., Li, C., Marton, I., 2021. SARS-CoV-2 variant prediction and antiviral drug design are enabled by RBD in vitro evolution. Nat. Microbiol. 6 (9), 1188–1198.

Zhao, Y., Bouffier, L., Xu, G., Loget, G., Sojic, N., 2022. Electrochemiluminescence with semiconductor (nano) materials. Chem. Sci. 13 (9), 2528–2550.

Zukauskas, S., Rucinskiene, A., Ratautaite, V., Ramanaviciene, A., Pilvenyte, G., Bechelany, M., Ramanavicius, A., 2023. Electrochemical biosensor for the determination of specific antibodies against SARS-CoV-2 spike protein. Int. J. Mol. Sci. 24 (1), 718.